Cell PRESS
Structure
Article

The Macromolecular Architecture of Extracellular Domain of αNRXN1: Domain Organization, Flexibility, and Insights into *Trans*-Synaptic Disposition

Davide Comoletti,[1,6,*] Meghan T. Miller,[1,6] Cy M. Jeffries,[3] Jennifer Wilson,[1] Borries Demeler,[4] Palmer Taylor,[1] Jill Trewhella,[3,5] and Terunaga Nakagawa[2,*]
[1]Department of Pharmacology, Skaggs School of Pharmacy and Pharmaceutical Sciences
[2]Department of Chemistry and Biochemistry
University of California, San Diego, La Jolla, CA 92093, USA
[3]School of Molecular Bioscience, University of Sydney, Sydney, NSW 2006, Australia
[4]Department of Biochemistry, The University of Texas Health Science Center, San Antonio TX 78229, USA
[5]Department of Chemistry, University of Utah, Salt Lake City, UT 84112, USA
[6]These authors contributed equally to this work
*Correspondence: dcomolet@ucsd.edu (D.C.), nakagawa@ucsd.edu (T.N.)
DOI 10.1016/j.str.2010.06.005

SUMMARY

Neurexins are multidomain synaptic cell-adhesion proteins that associate with multiple partnering proteins. Genetic evidence indicates that neurexins may contribute to autism, schizophrenia, and nicotine dependence. Using analytical ultracentrifugation, single-particle electron microscopy, and solution X-ray scattering, we obtained a three-dimensional structural model of the entire extracellular domain of neurexin-1α. This protein adopts a dimensionally asymmetric conformation that is monomeric in solution, with a maximum dimension of ~170 Å. The extracellular domain of α-neurexin maintains a characteristic "Y" shape, whereby LNS domains 1–4 form an extended base of the "Y" and LNS5-6 the shorter arms. Moreover, two major regions of flexibility are present: one between EGF1 and LNS2, corresponding to splice site 1, another between LNS5 and 6. We thus provide the first structural insights into the architecture of the extracellular region of neurexin-1α, show how the protein may fit in the synaptic cleft, and how partnering proteins could bind simultaneously.

INTRODUCTION

Genes encoding neuronal cell-adhesion proteins are essential for development and maintenance of connectivity in the nervous system. Synaptic cell-adhesion proteins constitute a principal pathway contributing to genetic susceptibility of autism spectrum disorders (ASD) (Geschwind and Levitt, 2007). Emerging evidence indicates that variations in copy number and other rare variants within the genes encoding neurexin-1 and -3 (*NRXN1* and *NRXN3*) contribute to ASD susceptibility and mental retardation (Feng et al., 2006; The Autism Genome Project Consortium, 2007; Kim et al., 2008; Yan et al., 2008; Glessner et al., 2009; Zahir et al., 2008; Zweier et al., 2009).

Neurexin-1α (αNRXN1) is a neuronal cell surface receptor that was originally identified as a high-affinity receptor for the spider toxin α-latrotoxin, whereas NRXN2 and 3 were subsequently identified from DNA sequence similarity with αNRXN1. Within each *NRXN* gene, the presence of two promoters, α and β, enables the expression of a longer α and a shorter βNRXN, yielding a total of six NRXN proteins (Missler and Südhof, 1998). Extensive independent alternative splicing of the encoded proteins (Ullrich et al., 1995) could specify a code of interactions between NRXNs and their ligands in different classes of synapses. Moreover, alternative splicing in NRXN3 creates a large diversity of secreted gene products, including those encoding multiple variants with in-frame stop codons (Ushkaryov and Südhof, 1993; Ullrich et al., 1995). Similar to the construct used in this study, all secreted splice variants end between the sixth Laminin, Neurexin, Sex-hormone-binding globulin (LNS) domain and various positions before the beginning of the transmembrane domain.

Currently, four groups of endogenous ligands for α and βNRXNs have been identified: neuroligins (NLGN) (Ichtchenko et al., 1995), neurexophilins (Missler et al., 1998), dystroglycan (Sugita et al., 2001), and leucine-rich repeat transmembrane proteins (LRRTM2) (de Wit et al., 2009; Ko et al., 2009). NRXNs and NLGNs are thought to form a *trans*-synaptic complex meeting near the center of the synaptic cleft, with the C-terminal sequences of either protein extending in opposite directions, tethering them to the pre- and postsynaptic membranes, respectively (Comoletti et al., 2007; Fabrichny et al., 2007; Araç et al., 2007; Chen et al., 2008). Early studies of cell association with neurons in cell culture suggested that NLGNs and NRXNs are sufficient to induce formation of new synapses (Scheiffele et al., 2000; Graf et al., 2004). In particular, all three αNRXNs induce clustering of the GABAergic postsynaptic scaffolding protein gephyrin and NLGN2, but not of the glutamatergic postsynaptic scaffolding protein PSD-95 or NLGN 1/3/4 in an artificial synapse-formation assay (Kang et al., 2008). This suggests that αNRXNs may be mediators of GABAergic synaptic protein

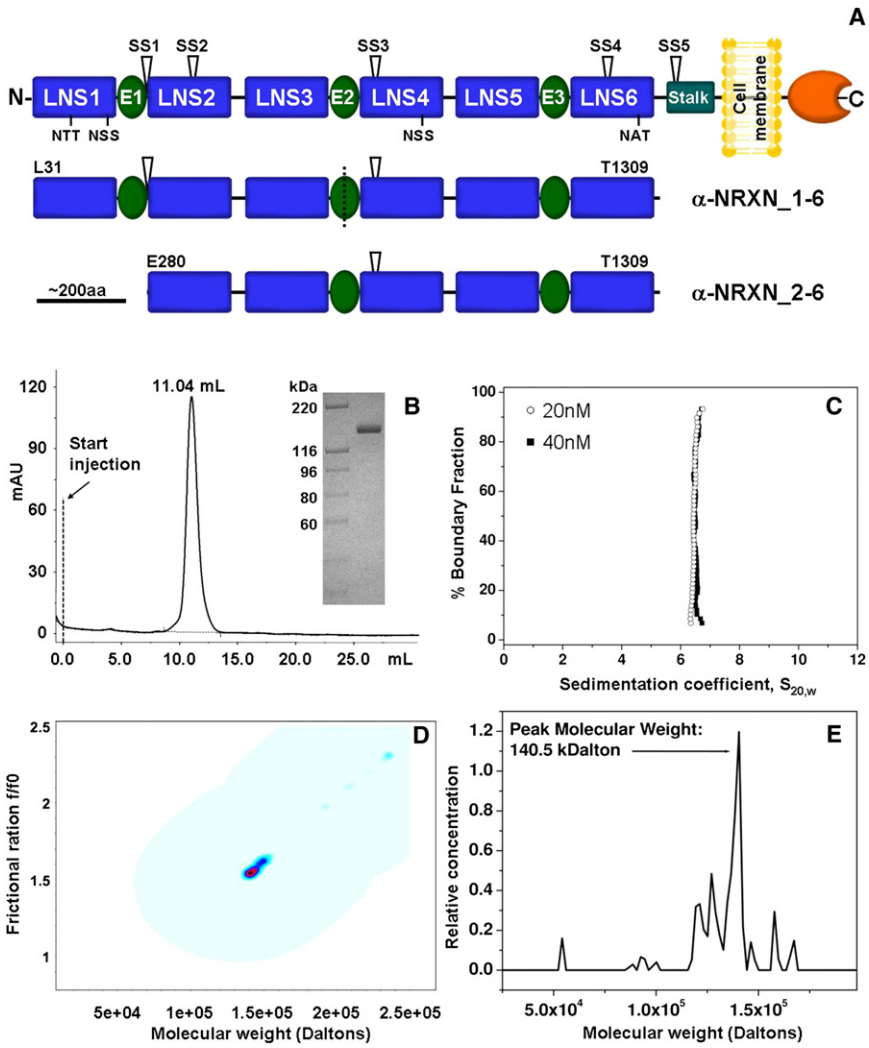

Figure 1. Schematic Diagram of the αNRXN1 Constructs Used and Hydrodynamic Characterization of the Purified Extracellular Domain of αNRXN_1-6

(A) Top: the domain organization of full-length αNRXN1 with respect to the pre-syanptic membrane. The C-terminal intracellular domain is shown to the right of the membrane, whereas the large N-terminal region extending into the synaptic cleft is shown on the left. Stalk, O-lined glycosylated domain; E1 to E3, EGF domains. Potential N-linked glycosylation sites are indicated using single letter code; open arrowheads , sites alternative splicing. Bottom: the extracellular regions of the αNRXN1 used for this study. L31, E280, and T1309 refer to the amino acid number in the protein sequence. The dotted line indicates a potential center of symmetry.

(B) Size exclusion chromatography trace of purified αNRXN_1-6. Inset, Coomassie blue staining of a sample composed of the main peak.

(C) G(s) distribution plots from the enhanced van Holde–Weischet analysis of sedimentation velocity experiments of two concentrations of αNRXN_1-6.

(D) Two-dimensional spectrum/Monte Carlo analysis of the 20 nM velocity experiment. The distribution shows a single, monomeric species with a molecular weight of ~140 kDa. The blue gradient indicates partial concentration.

(E) Concentration histogram of the globally fitted fixed molecular weight distribution analysis of the sedimentation equilibrium data. See also Figure S1.

recruitment and stabilization. Earlier studies of αNRXN-knockout mice revealed only mild variations in synaptic density and ultrastructure (Dudanova et al., 2007). More recently, a study of the αNRXN-1 knockout showed severe impairment of excitatory neurotransmission pathways (Etherton et al., 2009). αNRXNs appear to play a functional role at the synapse, including mediating Ca^{2+}-triggered neurotransmitter release (Missler et al., 2003), but do not seem to participate in synapse formation. These findings suggest that the αNRXNs are a group of *trans*-synaptic cell-adhesion molecules that participate in a modular organization of presynaptic terminals by mediating the localized activation of Ca^{2+} channels.

Structurally, αNRXN1 is a large (~160 kDa) multidomain protein composed of several discernable regions. A cleavable N-terminal signal peptide is responsible for trafficking the protein to the cell membrane. The mature protein contains three homologous repeats, each motif composed of a central epidermal growth factor (EGF) domain flanked upstream and downstream by two LNS domains sharing limited protein identity (Figure 1A). These three repeats, formed by nine independently folded domains that span ~90% of the protein sequence, are followed by a single stalk domain that is likely to be partially rigidified through extensive O-linked glycosylation. The stalk domain connects to a single transmembrane domain and a short cytoplasmic tail containing a classical PDZ recognition motif that appears to target NRXN to the presynaptic region (Fairless et al., 2008). Although the crystal structures of the isolated second, fourth, and sixth LNS domains of αNRXN1 have been solved (Rudenko et al., 1999; Sheckler et al., 2006; Shen et al., 2008), the overall domain complexity of the intact protein has been an impediment to examining structural organization beyond individual LNS domains.

Using a set of complementary biophysical techniques, we developed a three-dimensional structural model of the entire extracellular domain of αNRXN1 in solution. Although some flexibility at the extremities of the extracellular domain is detected, the overall architecture of αNRXN1 is consistent with a semielongated protein with a stable shape resembling the letter "Y." The results reported here represent, to our knowledge, the first three-dimensional structural models of the extracellular domain of αNRXN super-family that include neurexin (1 to 3) and Caspr (Contactin associated-like protein) 1 to 5. Together, these results should facilitate the understanding of how αNRXN might be arranged in the limited space of the synaptic cleft and how this protein may associate with multiple transmembrane and soluble synaptic proteins.

RESULTS

Characterization of the Purified Extracellular Domain of αNRXN

Protein expression and N-terminal sequencing

Two constructs from the extracellular domain of αNRXN1 were expressed as soluble entities in the cell culture medium of HEK293 GnTI- cells: one starting at position Leu31 and encompassing sites of alternative splicing #1 and #3 (αNRXN_1-6) and an N-terminal deletion devoid of the first LNS and EGF domains to yield a protein starting at position Glu280 (αNRXN_2-6) (Figure 1A). By size exclusion chromatography, both constructs elute as single peaks (see Figure 1B; see Figure S1A available online), indicating the presence of homogeneous monomeric species. In SDS-PAGE followed by Coomassie blue staining, αNRXN_1-6 and αNRXN_2-6 appear as single bands of ~140 kDa and ~110 kDa (insets of Figure 1B; Figure S1A), consistent with the calculated molecular weight of the peptides. As we express αNRXN protein with its native leader peptide (mgtallqrggcfllclslllllgcwaelgsgLEFPG), Edman degradation of the first five residues of the mature protein was performed to assign the initial amino acids after the cleavage of the leader sequence. The unambiguously determined sequence Leu-Glu-Phe-Pro-Gly indicated that the mature protein starts at Leu31, consistent with previous findings (Missler et al., 1998) and sequence predictions.

Mass spectrometric analysis of αNRXN

Both αNRXN1 constructs were expressed in the culture medium of HEK293 GnTI- cells. These cells lack N-acetylglucosaminyltransferase I (GnTI) activity, and consequently glycosylation remains restricted to a homogeneous seven-residue oligosaccharide (Reeves et al., 2002), thus simplifying structural analyses. αNRXN1 contains four potential N-linked glycosylation sites at positions N125, N190, N790, and N1223 (Figure 1). Although the peptidic mass of the expressed protein is calculated to be 140,619 Da, MALDI-TOF indicated a MW value of 145,896 Da (data not shown) with a difference of 5278 Da between the two values. Because GnTI-cells only add to each N-linked glycosylation site a Man5GlcNAc2 (mass, 1361 Da), the estimated occupancy of the potential N-linked sugars is 3.87 units per molecule, a value consistent with conjugation by oligosaccharde at all four N-linked glycosylation sites. Functionally, αNRXN_1-6 is fully active in binding neuroligin-1 (Figure S1B) (Boucard et al., 2005) and LRRTM2 (de Wit et al., 2009).

Analytical Ultracentrifugation Analyses of the Extracellular Domain of αNRXN1

Sedimentation velocity and equilibrium measurements provide complementary information useful in determining the globularity and oligomerization state of the extracellular domain of αNRXN1 in solution. To determine whether αNRXN_1-6 forms reversibly self-associating oligomers, we compared sedimentation coefficient distributions extracted using the enhanced van Holde–Weischet analysis (Demeler and van Holde, 2004) of two different loading concentrations. This analysis shows identical monodisperse species for both concentrations (Figure 1C), suggesting an absence of oligomerization at these concentrations. The same data were then analyzed by Monte Carlo analysis (Demeler and Brookes, 2008) together with a two-dimensional spectrum analysis (Brookes et al., 2010) and genetic algorithm analysis (Brookes and Demeler, 2007) to establish a molecular weight (Figure 1D). These analyses indicated that αNRXN_1-6 has a sedimentation coefficient of 6.36 s (6.28 s, 6.39 s) and a molecular weight of 141 kDa (136.5 kDa, 151.4 kDa), with a frictional ratio of 1.54 (1.51, 1.64), consistent with the monomeric mass of αNRXN and indicative of an elongated particle (values in parenthesis are 95% confidence intervals from the Monte Carlo analysis) (Demeler, 2009). The monomeric molecular weight was confirmed by sedimentation equilibrium data and a fixed molecular weight distribution analysis that gave a peak molecular weight of ~140 kDa (Figure 1E). Both sedimentation velocity and equilibrium experiments were in excellent agreement with the expected molecular weight based on amino acid sequence and mass spectrometry analyses.

Single Particle Electron Microscopy

αNRXN_1-6

To obtain structural information on the extracellular domain of αNRXN1, the purified protein was negative-stained and imaged using a transmission EM. αNRXN_1-6 particles were monodisperse and homogeneous in size, although individual particles adopted a variety of conformations (Figure 2A). Approximately 6,000 particles were analyzed using multivariate statistics, image classification, and averaging. In the majority of the class averages, only five globular domains were clearly visible. We presumed that only five of the six LNS domains were uniformly aligned because of extensive conformational heterogeneity intrinsic to the particles (Figure 2B). Analysis of the SDS-PAGE profiles (data not shown) indicated that the protein was intact, and careful inspection of the raw particle images indicate that all six domains were always detectable but appear faintly only in a few class averages (Figure 2C). We concluded that the missing domain was poorly averaged because of its extensive flexibility. These observations provide direct evidence that the LNS1-EGF1 tandem is extremely mobile, because of the flexible linkage of the LNS1 domain respect to the more rigid bulk of the molecule. Molecular labeling was conducted to deduce the N- to C-terminal orientation of the protein. We introduced a FLAG tag at the N terminus and an HA tag at the C terminus and labeled the purified protein with the antigen-binding fragment (Fab) against each of the epitope tags separately. The images of the HA Fab-tagged αNRXN_1-6 particles identified the C terminus (LNS6) in the more structured triangular region (Figure 2D), whereas the FLAG Fab-tagged αNRXN_1-6 identify first LNS domain in the more elongated and flexible region (Figure 2D). Overall, single-particle EM reveals that the extracellular domain of αNRXN adopts a semielongated and asymmetric structure with a shape reminiscent of the letter Y. Although this labeling does not allow a positive identification of each LNS domain, by their sequence in the protein, we infer that LNS domains 1–4 form the longer base of the "Y" and LNS5-6 the two arms.

αNRXN_2-6

To reduce the large conformational flexibility in the molecule conferred by the first LNS domain, we removed the N-terminal portion of the protein, which included the first LNS and EGF domains, and the flexible linker region containing the alternative

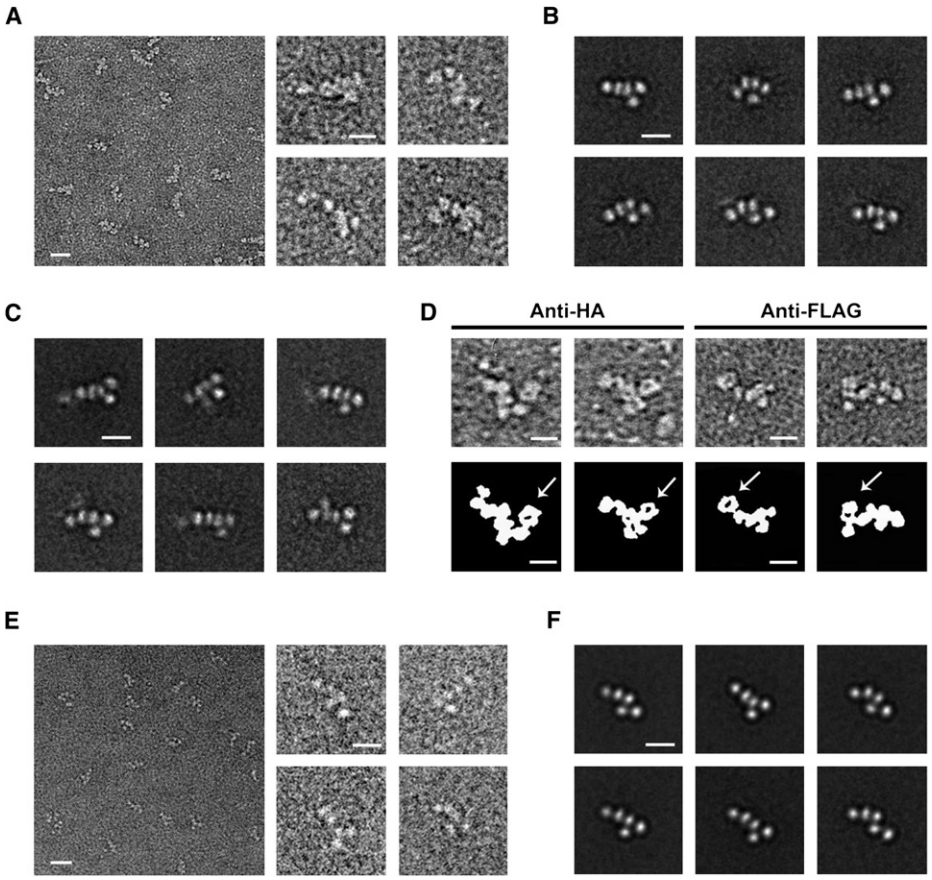

Figure 2. Single-Particle Electron Microscopy Characterization of αNRXN_1-6 and αNRXN_2-6

(A) Raw data images of the particles before alignment (left panel). Scale bar, 20 nm. Boxed particle, scale bar equals 10 nm.

(B) Selection of the highest represented class averages which show only five visibly distinct domains. The panels show the breadth of flexibility of the particles. Scale bar, 10 nm.

(C) Several averages with low representation indicate the presence of a sixth domain. Scale bar, 10 nm.

(D) Labeling of αNRXN 1-6 with Fab fragments against a C-terminal HA tag, and an N-terminal FLAG tag. Raw data images are above and a schematic representation with arrows pointing to the identified Fab fragment is below. Scale bar, 10 nm.

(E) Left panel, raw data of αNRXN_2-6 particles; 17,321 particles were aligned and grouped into 150 class averages. Scale bar, 20 nm.

(F) Six of the highest represented averages show various conformations. Scale bar, 10 nm. See also Figure S2.

splice site 1 (Figure 1A), generating a protein beginning at Glu280 (αNRXN_2-6). Approximately 17,000 particles of αNRXN_2-6 were analyzed, and 150 class averages were generated. The most common class averages clearly define all five LNS domains in αNRXN_2-6. By removing LNS1, our identification of the N and C termini was also confirmed: the particle alignment was greatly improved by the N-terminal truncation, and the structured triangular region was maintained (Figures 2E and 2F). The difference in particle shapes detectable in the class averages show that, although some flexibility remains at the junctions between LNS domains, the general Y shape is conserved. The class averages shown in Figure 2F depict the range of conformational variability. Although little variation is present at the N terminus of the protein, more flexibility is adopted at the C terminus where the Y shape can be disrupted by LNS6 being removed from LNS4. The complete set of class averages shown in Figure S2 yields a more comprehensive view of the conformational heterogeneity of the extracellular domain of αNRXN1. Probably because of their small size, densities corresponding to the three EGF domains remain unresolved. Overall, it appears that αNRXN1 has a tightly packed core composed of LNS2-4 and contains flexible regions that allow the extremities of the protein to extend and retract freely. From a biological perspective, this mobility could be relevant for allowing the domain to fit within the dimensions of the synaptic cleft and interact simultaneously with multiple binding partners. Having established the basic two-dimensional conformation of the extracellular domain of αNRXN1, we proceeded to reconstruct the three-dimensional structure using solution scattering methods.

Small Angle X-Ray Scattering Analysis of the Extracellular Domain of αNRXN1

Reproducible, high-quality scattering data for the entire extracellular domain of αNRXN_1-6 were collected from three independent sample preparations as well as from monodisperse solutions of lysozyme used as a secondary standard for

calibration of scattering intensity (Krigbaum and Kugler, 1970). Single-particle EM results show that the first LNS-EGF pair is significantly flexible. Therefore, to simplify our structural analyses and to strengthen our interpretation of the small angle X-ray scattering (SAXS) data, experiments on the truncated αNRXN_2-6 construct were also performed. The forward scattering intensities ($I(0)$) and radius of gyration (R_g) of each of the αNRXN_1-6 and αNRXN_2-6 samples were derived from the scattering data using Guinier analysis. As expected for monodisperse particles in solution, excellent linear correlations were observed in the Guinier plots for both constructs (Figure S3, top panels), and no significant concentration-dependent change in the R_g or $I(0)$ values were observed (Figure S3, lower panels). Using the known relationship $I(0)/c \propto$ MW (with c in units of mg/mL) and comparing data with that of lysozyme scattering, estimates of the molecular weight of the scattering particles were 164–174 kDa for αNRXN_1-6, and 109–118 kDa for αNRXN_2-6, consistent with hydrodynamic and mass spectrometric measurements (for detailed tabulated results of $I(0)$, R_g and molecular weight estimates, see Table S1).

Indirect Fourier transformation yields the probable interatomic distance distribution $P(r)$ within the scattering molecule, providing an estimate of the maximum dimension of the particle and its shape. The $P(r)$ profiles for αNRXN_1-6 and αNRXN_2-6 (Figure 3), calculated using the program GNOM (Svergun, 1992), indicate that both proteins (Figures 3B and D, respectively) are extended particles in solution (structurally anisotropic), as noted by the skewed distribution of vector lengths. The maximum dimension, D_{max}, of the full-length construct is ~170 Å with an average R_g of 53.0 ± 0.3 Å. As expected, the truncated variant is significantly smaller, with a D_{max} of ~145Å and an average R_g of 44.2 ± 0.6 Å. Removing the LNS-EGF pair shortens the maximum dimension of the protein by ~25 Å and decreases the radius of gyration of ~9 Å without altering the general shape of the $P(r)$ profile. Despite inherent segmental flexibility, the significantly shorter maximum dimension of the deletion mutant αNRXN_2-6 indicates that the domains within the LNS_2-6 region of the protein retain their extended configuration upon removal of the LNS1-EGF1 domain pair. Taken together, these data show that the extracellular domain of αNRXN is monomeric in solution and free of aggregation or interparticle interference. Thus, the scattering data fulfill the requirements necessary for extracting accurate shape information from which reliable three-dimensional structural models of αNRXN_1-6 and αNRXN_2-6 can be constructed.

Three-dimensional Reconstruction of the Extracellular Domain of αNRXN1

Using a combination of high-resolution structures and homology models of the individual LNS and EGF subunits, rigid-body modeling of the SAXS data enabled us to obtain independent three-dimensional structural models of αNRXN that closely resemble the shapes obtained with single-particle EM. The crystal structures of LNS 2, 4, and 6 are available (Rudenko et al., 1999; Sheckler et al., 2006; Shen et al., 2008), and homology models of the remaining individual subunits (LNS1, 3, and 5; EGF1, 2, and 3) were built using various high-resolution templates, as specified in Experimental Procedures. Eight sequences, ranging between 4 and 26 residues, linking various

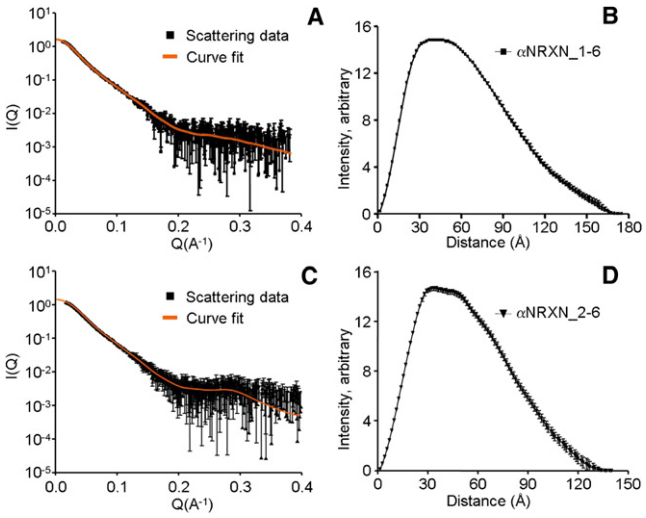

Figure 3. Scattering Intensity and *P(r)* Functions of the αNRXN_1-6 and αNRXN_2-6

(A and C) Scattering profiles of the highest concentrations of αNRXN_1-6 and 2-6 and *P(r)* fits.

(B and D) *P(r)* functions of αNRXN_1-6 and 2-6 proteins, indicating the maximum dimension of the particle. Statistical quality of the data in panels B and D can be assessed by the standard error bars; some estimated errors are smaller than the symbols. See also Table S1 and Figure S3.

LNS and EGF domains did not have a suitable three-dimensional template and thus were initially omitted from the calculations performed with the program SASREF (Petoukhov and Svergun, 2005). Distance constraints were imposed between the nine individual rigid bodies to ensure that the N and C termini of the individual domains remain within reasonable distances during refinement (details in Tables S2 and S3). The SASREF refinements were run multiple times against scattering intensity data from αNRXN_1-6 and αNRXN_2-6. The majority (~80%) of solutions converged toward a single class of Y-shaped molecule with LNS1/LNS2 forming the base of the Y and LNS5/LNS6 forming the arms (Figure 4), in excellent agreement with the EM images (Figure 2).

Approximately 11% of the mass of αNRXN_1-6 (primarily in the linkers connecting LNS1/EGF1 and EGF1/LNS2) was not included in the SASREF modeling, whereas only ~4% of the mass was missing for αNRXN_2-6. We therefore used the program BUNCH that, although similar to SASREF, can additionally account for contributions from regions of the model with unknown structure. Initial BUNCH refinements were performed using similar distance constrains as those used in SASREF against both αNRXN_1-6 and αNRXN_2-6 data sets and the fit to the data improved for both constructs (Figure 4A) (further details on BUNCH refinement strategy are available in the Supplemental Information). As expected, all of the refined BUNCH models maintain the characteristic Y-shape obtained by the other methods. In addition, they show the likely average positioning of the linkers of unknown structure.

Because of the inherent flexibility of the multidomain architecture, although we present the "best-fit" SASREF and BUNCH models for both constructs (Figure 4A), it is most pertinent to

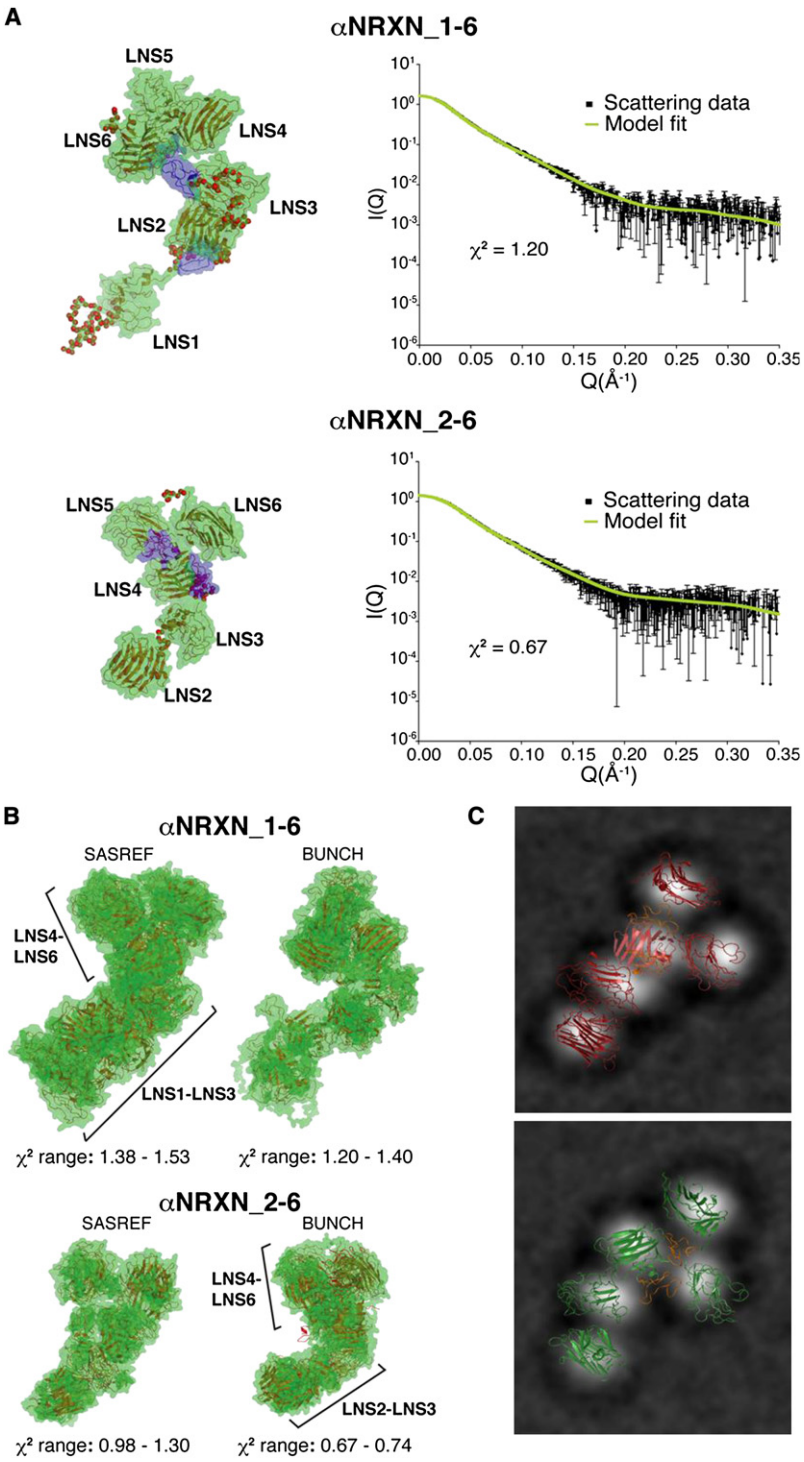

Figure 4. Rigid Body Modeling of the αNRXN_1-6 and 2-6 with the SAXS Data and αNRXN_2-6 SAXS Models Overlay on Selected EM particles

(A) Best-fit models of αNRXN_1-6 and αNRXN_2-6 derived from BUNCH rigid-body refinement and their respective fits to the data. The EGF domains are colored blue (EGF3 is occluded in αNRXN_1-6).

(B) Structural ensembles represented as semitransparent green surfaces and ribbons of both αNRXN constructs generated using SASREF and BUNCH rigid body modeling. Brackets indicate different domains of the ensemble. For clarity, brackets and domain labels have been omitted for some ensembles.

(C) Green and red are two different SASREF reconstructions manually superimposed to two similar class averages to show their degree of identity. Atomic models were made using PyMol (http://www.pymol.org). See also Tables S2 and S3.

view the results in terms of ensembles of structures that share a common Y-shaped topology (Figures 2 and 4B). For example, the arms of the Y (LNS5 or LNS6) can be spatially swapped without greatly affecting the general Y-shape of the model. Furthermore, upon comparing each member across the SASREF and BUNCH ensembles, the individual domains can undergo a limited localized tilting or rotation relative to their domain neighbors without affecting the fits to the data. Consequently, although the general architecture of the protein is maintained, the RMSD C_α across the ensembles is broad, ranging from ~7 to 25 Å. Although this variability could be due to inherent limitations in modeling a protein with multiple domains, the solution scattering results are consistent with the electron microscopy data that indicate individual domains can reorient via flexible interdomain linkers.

DISCUSSION

The small volumes and spanning dimensions of synaptic clefts are critical for rapidity and fidelity of synaptic transmission. With a typical span of ~24 nm between the pre- and postsynaptic membrane, it is unclear how large multi-domain proteins such αNRXN (~1400 amino acids in its entire extracellular domain), L1CAM (~1300 amino acids), and protocadherin (~1100 amino acids), along with other large synaptic receptors and channels, are structured to coexist within the cleft and maintain synaptic structure and function. Furthermore, the extracellular domains of these large proteins are generally composed of a sequential arrangement of several individually folded domains connected by flexible linkers, and they associate with multiple partnering proteins. Whether these proteins are completely flexible or have a restricted interdomain segmental motion is unknown. The αNRXNs are not only bulky multidomain molecules, but between the sixth LNS and transmembrane domains they contain a sequence of ~100 residues that is relatively rich in Ser and Thr and shown to be O-linked glycosylated (Ushkaryov et al., 1992). The presence of oligosaccharides, combined with a relative abundance of Pro residues, presumably rigidifies and elongates the peptide chain, as demonstrated in

neuroligin-1 and other cell-surface receptors (Li et al., 1996; Merry et al., 2003; Comoletti et al., 2007). The length of this single chain tether may be advantageous to extend the sixth LNS domain so that it can approach the center of the synaptic space, permitting association with postsynaptic proteins such as neuroligin or LRRTM2 (Comoletti et al., 2007; de Wit et al., 2009; Ko et al., 2009). The presence of the stalk domain, however, extends the overall length of αNRXN beyond what a semielongated amino acid sequence would predict.

Sedimentation velocity and equilibrium analyses unambiguously show that the extracellular domain of αNRXN is a semielongated monomer. Although analytical ultracentrifugation experiments employ low protein concentration (between 10 nM and 7 μM, equivalent to 0.0014 and 1 mg/mL, respectively) that could favor dissociation to the monomeric species, SAXS experiments were conducted at concentrations up to ~6 mg/mL (~40 μM). Under these conditions, higher order oligomers were not detected, indicating that the extracellular domain of αNRXN, similar to β-neurexin (Comoletti et al., 2006), does not self-associate. Thus, unless oligomerization occurs through the short intracellular domain, αNRXN is likely present as a monomer on the cell surface.

Single-particle EM shows that the LNS1-EGF1 pair of αNRXN_1-6 has extensive interdomain flexibility with respect to the rest of the protein. This flexibility is likely due to the length of the linker (27 amino acids, S256–Y282) that contains splice insert 1. Conversely, the excellent averaging of the particles for αNRXN_2-6 indicates that the rest of the molecule maintains a more stable conformation (Figure 2). The central region of the protein shows LNS2 to 4 in a linear arrangement, whereas LNS5 lies at various angles in relation to the previous domains. LNS6 normally folds back on the protein, making a triangular or Y shaped arrangement with LNS4, but displays a large degree of flexibility.

Building on the crystal structures of LNS domains 2, 4, and 6 (Rudenko et al., 1999; Sheckler et al., 2006; Shen et al., 2008) and from homology models for the remaining domains, we constructed three dimensional structures of the entire extracellular domain of αNRXN1, including the linker regions, and optimized them against X-ray solution scattering data. Consistent with hydrodynamic and electron microscopy findings, the three dimensional best-fit models show that αNRXN maintains a semielongated structure, with LNS domains 1–4 arranged linearly and LNS 4, 5, and 6 adopting a triangular "clover leaf" conformation (Figure 4). Scattering data record the time and rotationally averaged structural information from molecules in solution, rather than a "snap shot" of a single molecule on a grid as it is observed by EM. The rotational averaging inherent to the solution scattering experiment reduces the information content to one-dimension and thus, when interpreting three-dimensional models, some basic starting assumptions must be satisfied. First, on comparing the $P(r)$ profiles of αNRXN_1-6 and αNRXN_2-6 and from a direct overlay of the scattering data, a level of structural preservation must be maintained within the LNS2-LNS6 region of the protein that is not affected by the removal of the LNS1-EGF1 domain pair. Second, in the jelly roll fold of the LNS domain the metal-binding pocket, where neuroligins bind, is located at the rim of the β sheet sandwich opposite the N and C termini (Rudenko et al., 1999) that reside close together. Consequently when one LNS domain is connected to the next (or to an EGF domain) by relatively short ~5–7 amino acid linkers, as in the case of the LNS4-6, these domains will be constrained toward a "clover leaf" spatial arrangement as opposed to a linear "beads on a string" conformation (Tisi et al., 2000; Carafoli et al., 2009). Third, although the extracellular domain of αNRXN_1-6 could be considered symmetrical with EGF2 at the center of a two-fold symmetry (Figure 1A), the N and C termini identification with Fab tagging and the deletion construct αNRXN_2-6 yields a precise orientation of the protein. Together, the three-dimensional reconstructions and electron microscopy micrographs show extensive interaction between domains 2, 3, and 4, thus explaining the relative rigidity of this part of the molecule. Consistent with the higher degree of flexibility evident in the raw particle images in the EM micrographs, fewer contacts appear between LNS1 and 2 and between LNS5 and 6. Together, these results indicate that the protein maintains a stable core architecture that likely exists in an extracellular milieu and anchors its biological functions (Figure 5).

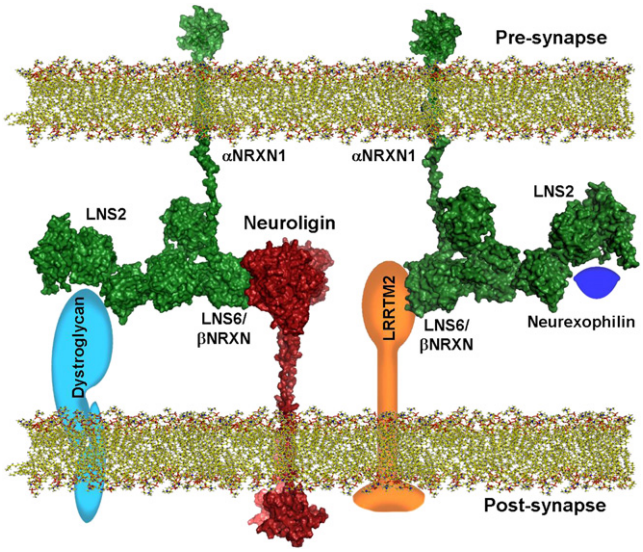

Figure 5. Schematic Model of the Complex Between αNRXN and its Ligands in the Context of the Synapse

The αNRXN stalk domain connects the presynaptic membrane to LNS6 of one of the structural models obtained with SASREF. Information on the contact surface between NLGN and LNS6 of αNRXN was taken from the available crystal structure. Stalk domains are drawn extended because of their likely semirigid structure. Intracellular domains of both NLGN and NRXN have no conformational assignment. Schematic models of the other known αNRXN ligands (dystroglycan, neurexophilin, and LRRTM2) are added to show how multiple ligands can associate simultaneously to their respective LNS domains. Structural models have depth cue visual information. Approximate distances and dimensions are to scale (pre- and postsynaptic gap is maintained at ~22 nm).

Proteins comprising a large number of independently folded domains, such as the αNRXN, laminin-G, and others are normally flexible because interdomain motions are likely linked to their biological activities. The high-resolution structure of LNS 1-3 of laminin α2 (Carafoli et al., 2009) shows that inter-LNS domain linkers maybe extended and flexible. In the case of αNRXN, multiple interacting proteins have been isolated and

characterized. In particular, neurexophilin appears to bind to the second LNS domain of αNRXN (Missler et al., 1998), whereas the neuroligins and LRRTM2 associate with the sixth LNS domain (Ichtchenko et al., 1995; Boucard et al., 2005; de Wit et al., 2009; Ko et al., 2009) and dystroglycan associates with both the second and the sixth LNS domains (Sugita et al., 2001). The mobility of LNS1 provides greater surface accessibility to the second LNS domain. LNS6, belonging to the arms of the "Y" shape, tends to fold back toward LNS4, creating a more compact structure, potentially limiting the accessibility to binding partners (Reissner et al., 2008). However, single-particle EM data show that LNS6 retains some flexibility, and the clover-leaf arrangement suggests that the metal binding rim of each LNS domain is likely solvent exposed rather than being confined to interdomain stabilization. Regarding the decreased affinity that αNRXN shows with the neuroligins (Boucard et al., 2005), it is possible that the extensive flexibility and segmental motion of LNS6 may require that optimal binding is achieved only after a conformational change, thus acting as a factor limiting NLGN binding.

The three-dimensional structural models of αNRXN we present here are, to our knowledge, the first experimentally derived models of the entire extracellular domain of the αNRXN super-family or other LNS modular multidomain proteins. Taking advantage of the multiple crystal structures available of the complex between neuroligin 1 and 4 (Fabrichny et al., 2007; Araç et al., 2007; Chen et al., 2008) with βNRXN, and using our previous findings on the structure of the stalk domain of the neuroligins, we assembled a model of the complex between one of the αNRXN_1-6 models and neuroligin 1 in the context of the synaptic cleft. In the case of αNRXN, flexibility, partial elongation, and the clover-leaf arrangement of LNS4-6 domains are ideal for binding multiple ligands because each LNS subunit can associate with partnering proteins independent of the neighboring domains. As shown in the model of the complex (Figure 5), the presence of the stalk region and the elongated nature of this model explain how multiple ligands can bind simultaneously to the extracellular domain of αNRXN, and how it may orient in the synaptic cleft.

As hypothesized in an earlier work (Tabuchi and Südhof, 2002), mutations in *NRXN* genes likely confer subtle phenotype changes that may result in widespread dysfunction during the development of a complex nervous system, particularly in a polygenic disorder involving other proteins affecting neuronal system development. In fact, new evidence indicates that variations in copy number and rare variants within the genes encoding neurexin-1 and -3 (*NRXN1* and *NRXN3*) contribute to ASD susceptibility, mental retardation (Feng et al., 2006; The Autism Genome Project Consortium, 2007; Kim et al., 2008; Yan et al., 2008; Glessner et al., 2009), schizophrenia (Rujescu et al., 2009), and in altering addiction and reward behaviors to nicotine (Nussbaum et al., 2008).

EXPERIMENTAL PROCEDURES

Expression of αNRXN1

The construct encoding the secreted, soluble extracellular domain of αNRXN1 IgG fusion protein (Ig-N1α-1) (Boucard et al., 2005) was a kind gift of Dr. Thomas Südhof (Stanford, CA). We adapted this construct by introducing a 3C protease cleavage site (LEVLFQ/GP) between residue T1309 of αNRXN and the beginning of the hIgG sequence. HEK293 GnTI cells were transfected with the appropriate plasmids and were selected by growth in G418 (Geneticin, Sigma) (Comoletti et al., 2003). For protein expression, cells were maintained at 37°C and 10% CO_2 in Dulbecco's modified Eagle's medium containing up to 2% fetal bovine serum.

Analytical Ultracentrifugation

All analytical ultracentrifugation experiments were performed in a Beckman/Coulter XL-I ultracentrifuge using An60Ti and An50Ti rotors at the Center for Analytical Ultracentrifugation of Macromolecular Assemblies, San Antonio, TX. Sedimentation equilibrium and velocity experiments were analyzed with the UltraScan software, version 9.9, release 847 (Demeler, 2009). All samples were run in 10 mM sodium phosphate buffer (pH 7.4) with 137 mM NaCl and 2.7 mM KCl, at 4°C. Hydrodynamic corrections were made according to Laue et al. (1992) as implemented in UltraScan.

Negative-Stain Single-Particle Electron Microscopy

Purified αNRXN1 (0.05–0.1 mg/ml) in 10 mM HEPES (pH 7.4) and 150 mM NaCl solution was applied to glow-discharged carbon-coated grids and was negatively stained with 0.75% uranyl formate, as described elsewhere (Ohi et al., 2004). EM images for class averages were collected using an FEI 200KV Sphera microscope equipped with an LaB_6 electron filament using low-dose procedures on SO-163 Kodak film at a magnification of 50,000× and nominal defocus of −1.5 μm. Micrographs were digitized with a Nikon scanner, and particles were selected interactively using the WEB display program. A second pass selection of properly centered particles was done interactively, and particles were aligned and classified by reference-based alignment and the K-means classification (100–150 classes) using the SPIDER suite (Frank et al., 1996).

Small-Angle X-Ray Scattering Data Acquisition of αNRXN1

Data were collected from the proteins and their solvent blanks (ultrafiltrate buffers for the αNRXN and last step dialysate for lysozyme) at 20°C, using an Anton Paar SAXSess line collimation instrument at the University of Utah on 2D position-sensitive image plates (10 mm slit and integration width) as described by Jeffries et al. (2008).

Structure Modeling from the Scattering Data

Rigid body modeling was performed using the programs SASREF and BUNCH (Petoukhov and Svergun, 2005). Both techniques refine the domain positions within the protein against the scattering data using calculated partial scattering amplitudes derived from the atomic structures of the individual component domains.

More information on some of the methods can be found in the Supplemental Information.

SUPPLEMENTAL INFORMATION

Supplemental Information includes three figures, three tables, and Supplemental Experimental Procedures and can be found with this article online at doi:10.1016/j.str.2010.06.005.

ACKNOWLEDGMENTS

This work was supported by USPHS (grant R37 GM-18360 to P.T.), NIEHS (grant P42ES10337 to P.T.), U.S. Department of Energy (grant DE-FG02-05ER64026 to J.T.), Autism Speaks (grant 2617 to D.C.), and the John Merck Fund and Hellman Foundation (support to T.N.). We acknowledge the use of the UCSD Cryo-Electron Microscopy Facility which was supported by NIH grants 1S10RR20016 and GM033050 to Timothy S. Baker and a gift from the Agouron Institute to UCSD. AUC supercomputer analyses were supported by NSF Teragrid allocation TG-MCB070038 (B.D.). UltraScan development is supported by NIH-RR022000 (B.D.). Calculations on Lonestar were supported by NSF TeraGrid allocation TG-MCB070038 (BD). We thank Dennis Winge (University of Utah, UT) for quantitative amino acid analysis, and Majid Ghassemian, Department of Chemistry and Biochemistry, for MALDI-TOF analysis. We thank A. G. Porter of the National University of Singapore for the kind gift of the 3C protease plasmid. We thank Michael Baker (Protein Data Bank) for

helpful discussion on homology modeling, and Greg Fuchs for excellent technical help during the preparation of the cleavable αNRXN construct.

Received: March 20, 2010
Revised: June 14, 2010
Accepted: June 17, 2010
Published: August 10, 2010

REFERENCES

Araç, D., Boucard, A.A., Ozkan, E., Strop, P., Newell, E., Südhof, T.C., and Brunger, A.T. (2007). Structures of neuroligin-1 and the neuroligin-1/neurexin-1 beta complex reveal specific protein-protein and protein-Ca2+ interactions. Neuron *56*, 992–1003.

The Autism Genome Project Consortium. (2007). Mapping autism risk loci using genetic linkage and chromosomal rearrangements. Nat. Genet. *39*, 319–328.

Boucard, A.A., Chubykin, A.A., Comoletti, D., Taylor, P., and Südhof, T.C. (2005). A splice code for trans-synaptic cell adhesion mediated by binding of neuroligin 1 to alpha- and beta-neurexins. Neuron *48*, 229–236.

Brookes, E., Cao, W., and Demeler, B. (2010). A two-dimensional spectrum analysis for sedimentation velocity experiments of mixtures with heterogeneity in molecular weight and shape. Eur. Biophys. J. *39*, 405–414.

Brookes, E., and Demeler, B. (2007). Parsimonious regularization using genetic algorithms applied to the analysis of analytical ultracentrifugation experiments. GECCO Proceedings ACM 978-1-59593-697-4/07/0007.

Carafoli, F., Clout, N.J., and Hohenester, E. (2009). Crystal structure of the LG1-3 region of the laminin alpha2 chain. J. Biol. Chem. *284*, 22786–22792.

Chen, X., Liu, H., Shim, A.H., Focia, P.J., and He, X. (2008). Structural basis for synaptic adhesion mediated by neuroligin-neurexin interactions. Nat. Struct. Mol. Biol. *15*, 50–56.

Comoletti, D., Flynn, R., Jennings, L.L., Chubykin, A., Matsumura, T., Hasegawa, H., Südhof, T.C., and Taylor, P. (2003). Characterization of the interaction of a recombinant soluble neuroligin-1 with neurexin-1beta. J. Biol. Chem. *278*, 50497–50505.

Comoletti, D., Flynn, R.E., Boucard, A.A., Demeler, B., Schirf, V., Shi, J., Jennings, L.L., Newlin, H.R., Südhof, T.C., and Taylor, P. (2006). Gene selection, alternative splicing, and post-translational processing regulate neuroligin selectivity for beta-neurexins. Biochemistry *45*, 12816–12827.

Comoletti, D., Grishaev, A., Whitten, A.E., Tsigelny, I., Taylor, P., and Trewhella, J. (2007). Synaptic arrangement of the neuroligin/beta-neurexin complex revealed by X-ray and neutron scattering. Structure *15*, 693–705.

Demeler, B. (2009) UltraScan version 9.9, release 847. Analytical ultracentrifugation data analysis software. The University of Texas Health Science Center at San Antonio, Dept. of Biochemistry. http://www.ultrascan.uthscsa.edu

Demeler, B., and van Holde, K.E. (2004). Sedimentation velocity analysis of highly heterogeneous systems. Anal. Biochem. *335*, 279–288.

Demeler, B., and Brookes, E. (2008). Monte Carlo analysis of sedimentation experiments. Prog. Colloid Polym. Sci. *286*, 129–137.

de Wit, J., Sylwestrak, E., O'Sullivan, M.L., Otto, S., Tiglio, K., Savas, J.N., Yates, J.R., 3rd, Comoletti, D., Taylor, P., and Ghosh, A. (2009). LRRTM2 interacts with Neurexin1 and regulates excitatory synapse formation. Neuron *64*, 799–806.

Dudanova, I., Tabuchi, K., Rohlmann, A., Südhof, T.C., and Missler, M. (2007). Deletion of alpha-neurexins does not cause a major impairment of axonal pathfinding or synapse formation. J. Comp. Neurol. *502*, 261–274.

Etherton, M.R., Blaiss, C.A., Powell, C.M., and Südhof, T.C. (2009). Mouse neurexin-1alpha deletion causes correlated electrophysiological and behavioral changes consistent with cognitive impairments. Proc. Natl. Acad. Sci. USA *106*, 17998–18003.

Fabrichny, I.P., Leone, P., Sulzenbacher, G., Comoletti, D., Miller, M.T., Taylor, P., Bourne, Y., and Marchot, P. (2007). Structural analysis of the synaptic protein neuroligin and its beta-neurexin complex: determinants for folding and cell adhesion. Neuron *56*, 979–991.

Fairless, R., Masius, H., Rohlmann, A., Heupel, K., Ahmad, M., Reissner, C., Dresbach, T., and Missler, M. (2008). Polarized targeting of neurexins to synapses is regulated by their C-terminal sequences. J. Neurosci. *28*, 12969–12981.

Feng, J., Schroer, R., Yan, J., Song, W., Yang, C., Bockholt, A., Cook, E.H., Jr., Skinner, C., Schwartz, C.E., and Sommer, S.S. (2006). High frequency of neurexin 1beta signal peptide structural variants in patients with autism. Neurosci. Lett. *409*, 10–13.

Frank, J., Radermacher, M., Penczek, P., Zhu, J., Li, Y., Ladjadj, M., and Leith, A. (1996). SPIDER and WEB: processing and visualization of images in 3D electron microscopy and related fields. J. Struct. Biol. *116*, 190–199.

Geschwind, D.H., and Levitt, P. (2007). Autism spectrum disorders: developmental disconnection syndromes. Curr. Opin. Neurobiol. *17*, 103–111.

Glessner, J.T., Wang, K., Cai, G., Korvatska, O., Kim, C.E., Wood, S., Zhang, H., Estes, A., Brune, C.W., Bradfield, J.P., et al. (2009). Autism genome-wide copy number variation reveals ubiquitin and neuronal genes. Nature *459*, 569–573.

Graf, E.R., Zhang, X., Jin, S.X., Linhoff, M.W., and Craig, A.M. (2004). Neurexins induce differentiation of GABA and glutamate postsynaptic specializations via neuroligins. Cell *119*, 1013–1026.

Ichtchenko, K., Hata, Y., Nguyen, T., Ullrich, B., Missler, M., Moomaw, C., and Südhof, T.C. (1995). Neuroligin 1: a splice site-specific ligand for beta-neurexins. Cell *81*, 435–443.

Jeffries, C.M., Whitten, A.E., Harris, S.P., and Trewhella, J. (2008). Small-angle X-ray scattering reveals the N-terminal domain organization of cardiac myosin binding protein C. J. Mol. Biol. *377*, 1186–1199.

Kang, Y., Zhang, X., Dobie, F., Wu, H., and Craig, A.M. (2008). Induction of GABAergic postsynaptic differentiation by alpha-neurexins. J. Biol. Chem. *283*, 2323–2334.

Kim, H.G., Kishikawa, S., Higgins, A.W., Seong, I.S., Donovan, D.J., Shen, Y., Lally, E., Weiss, L.A., Najm, J., Kutsche, K., et al. (2008). Disruption of neurexin 1 associated with autism spectrum disorder. Am. J. Hum. Genet. *82*, 199–207.

Ko, J., Fuccillo, M.V., Malenka, R.C., and Südhof, T.C. (2009). LRRTM2 functions as a neurexin ligand in promoting excitatory synapse formation. Neuron *64*, 791–798.

Krigbaum, W.R., and Kugler, F.R. (1970). Molecular conformation of egg-white lysozyme and bovine alpha-lactalbumin in solution. Biochemistry *9*, 1216–1223.

Laue, T.M., Shah, B.D., Ridgeway, T.M., and Pelletier, S.L. (1992). Analytical Ultracentrifugation in Biochemistry and Polymer Science, S.E. Harding, A.J. Rowe, and J.C. Horton, eds. (Cambridge: Royal Society of Chemistry).

Li, F., Erickson, H.P., James, J.A., Moore, K.L., Cummings, R.D., and McEver, R.P. (1996). Visualization of P-selectin glycoprotein ligand-1 as a highly extended molecule and mapping of protein epitopes for monoclonal antibodies. J. Biol. Chem. *271*, 6342–6348.

Merry, A.H., Gilbert, R.J., Shore, D.A., Royle, L., Miroshnychenko, O., Vuong, M., Wormald, M.R., Harvey, D.J., Dwek, R.A., Classon, B.J., et al. (2003). O-glycan sialylation and the structure of the stalk-like region of the T cell co-receptor CD8. J. Biol. Chem. *278*, 27119–27128.

Missler, M., and Südhof, T.C. (1998). Neurexins: three genes and 1001 products. Trends Genet. *14*, 20–26.

Missler, M., Hammer, R.E., and Südhof, T.C. (1998). Neurexophilin binding to alpha-neurexins: a single LNS domain functions as an independently folding ligand-binding unit. J. Biol. Chem. *273*, 34716–34723.

Missler, M., Zhang, W., Rohlmann, A., Kattenstroth, G., Hammer, R.E., Gottmann, K., and Südhof, T.C. (2003). Alpha-neurexins couple Ca^{2+} channels to synaptic vesicle exocytosis. Nature *423*, 939–948.

Nussbaum, J., Xu, Q., Payne, T.J., Ma, J.Z., Huang, W., Gelernter, J., and Li, M.D. (2008). Significant association of the neurexin-1 gene (NRXN1) with nicotine dependence in European- and African-American smokers. Hum. Mol. Genet. *17*, 1569–1577.

Ohi, M., Li, Y., Cheng, Y., and Walz, T. (2004). Negative staining and image classification—powerful tools in modern electron microscopy. Biol. Proced. Online *6*, 23–34.

Petoukhov, M.V., and Svergun, D.I. (2005). Global rigid body modeling of macromolecular complexes against small-angle scattering data. Biophys. J. *89*, 1237–1250.

Reeves, P.J., Callewaert, N., Contreras, R., and Khorana, H.G. (2002). Structure and function in rhodopsin: high-level expression of rhodopsin with restricted and homogeneous N-glycosylation by a tetracycline-inducible N-acetylglucosaminyltransferase I-negative HEK293S stable mammalian cell line. Proc. Natl. Acad. Sci. USA *99*, 13419–13424.

Reissner, C., Klose, M., Fairless, R., and Missler, M. (2008). Mutational analysis of the neurexin-neuroligin complex reveals essential and regulatory components. Proc. Natl. Acad. Sci. USA *105*, 15124–15129.

Rudenko, G., Nguyen, T., Chelliah, Y., Südhof, T.C., and Deisenhofer, J. (1999). The structure of the ligand-binding domain of neurexin Ibeta: regulation of LNS domain function by alternative splicing. Cell *99*, 93–101.

Rujescu, D., Ingason, A., Cichon, S., Pietiläinen, O.P., Barnes, M.R., Toulopoulou, T., Picchioni, M., Vassos, E., Ettinger, U., Bramon, E., et al. (2009). Disruption of the neurexin 1 gene is associated with schizophrenia. Hum. Mol. Genet. *18*, 988–996.

Scheiffele, P., Fan, J., Choih, J., Fetter, R., and Serafini, T. (2000). Neuroligin expressed in nonneuronal cells triggers presynaptic development in contacting axons. Cell *101*, 657–669.

Sheckler, L.R., Henry, L., Sugita, S., Südhof, T.C., and Rudenko, G. (2006). Crystal structure of the second LNS/LG domain from neurexin 1alpha: Ca2+ binding and the effects of alternative splicing. J. Biol. Chem. *281*, 22896–22905.

Shen, K.C., Kuczynska, D.A., Wu, I.J., Murray, B.H., Sheckler, L.R., and Rudenko, G. (2008). Regulation of neurexin 1beta tertiary structure and ligand binding through alternative splicing. Structure *16*, 422–431.

Sugita, S., Saito, F., Tang, J., Satz, J., Campbell, K., and Südhof, T.C. (2001). A stoichiometric complex of neurexins and dystroglycan in brain. J. Cell Biol. *154*, 435–445.

Svergun, D.I. (1992). Determination of the regularization parameter in indirect-transform methods using perceptual criteria. J. Appl. Cryst. *25*, 495–503.

Tabuchi, K., and Südhof, T.C. (2002). Structure and evolution of neurexin genes: insight into the mechanism of alternative splicing. Genomics *79*, 849–859.

Tisi, D., Talts, J.F., Timpl, R., and Hohenester, E. (2000). Structure of the C-terminal laminin G-like domain pair of the laminin alpha2 chain harbouring binding sites for alpha-dystroglycan and heparin. EMBO J. *19*, 1432–1440.

Ullrich, B., Ushkaryov, Y.A., and Südhof, T.C. (1995). Cartography of neurexins: more than 1000 isoforms generated by alternative splicing and expressed in distinct subsets of neurons. Neuron *14*, 497–507.

Ushkaryov, Y.A., and Südhof, T.C. (1993). Neurexin III alpha: extensive alternative splicing generates membrane-bound and soluble forms. Proc. Natl. Acad. Sci. USA *90*, 6410–6414.

Ushkaryov, Y.A., Petrenko, A.G., Geppert, M., and Südhof, T.C. (1992). Neurexins: synaptic cell surface proteins related to the alpha-latrotoxin receptor and laminin. Science *257*, 50–56.

Yan, J., Noltner, K., Feng, J., Li, W., Schroer, R., Skinner, C., Zeng, W., Schwartz, C.E., and Sommer, S.S. (2008). Neurexin 1alpha structural variants associated with autism. Neurosci. Lett. *438*, 368–370.

Zahir, F.R., Baross, A., Delaney, A.D., Eydoux, P., Fernandes, N.D., Pugh, T., Marra, M.A., and Friedman, J.M. (2008). A patient with vertebral, cognitive and behavioural abnormalities and a de novo deletion of NRXN1alpha. J. Med. Genet. *45*, 239–243.

Zweier, C., de Jong, E.K., Zweier, M., Orrico, A., Ousager, L.B., Collins, A.L., Bijlsma, E.K., Oortveld, M.A., Ekici, A.B., Reis, A., et al. (2009). CNTNAP2 and NRXN1 are mutated in autosomal-recessive Pitt-Hopkins-like mental retardation and determine the level of a common synaptic protein in Drosophila. Am. J. Hum. Genet. *85*, 655–666.